RESEARCH ARTICLE

VOLCANICA

How a non-harmonic-like tremor at a volcanic lake could be caused by sustained wind: A case of study of Taupō volcano

Henriette Bakkar*[α,β], Martha Savage[α], Finnigan Illsley-Kemp[α], and Eleanor R. H. Mestel[α]

[α] School of Geography, Environment, and Earth Science, Victoria University of Wellington, Wellington, New Zealand.
[β] Observatorio Vulcanológico y Sismológico de Costa Rica, Universidad Nacional, Heredia, Costa Rica.

Abstract

Taupō volcano lies underneath the largest lake in New Zealand. It undergoes unrest roughly every ten years, has minor eruptions every few hundred years, and has supereruptions. Understanding volcanic seismic signals provides insights into the volcano dynamics and helps to anticipate eruptions. Harmonic and non-harmonic volcanic tremor are common signals that indicate fluid mobilisation in volcanic systems. We observed a signal that resembled non-harmonic tremor during 2019 at Taupō volcano. Careful time-frequency analysis of seismic data and weather data from around the lake revealed that the signals were not magmatic in origin, but were most likely from lake microseisms caused by special conditions of the wind, which generates wind-driven waves in the lake. The frequency range of lake microseisms at Taupō starts and ends with a dominant frequency of 0.7–1.0 Hz, and during the maximum energy peak, the dominant frequency is of 0.50–0.56 Hz. Such signals may be common in caldera lakes, which need to be distinguished from tremor caused by volcanic activity, so as not to exaggerate the probability of eruptions.

Resumen

El volcán Taupō se encuentra bajo el lago más grande de Nueva Zelanda. Presenta periodos de inquietud volcánica aproximadamente cada diez años, tiene erupciones menores cada pocos cientos de años y super erupciones raramente. La comprensión de las señales sismo-volcánicas proporciona información sobre la dinámica del volcán y ayuda a la anticipación de las erupciones. El tremor armónico volcánico y no armónico son señales comunes que indican la movilización de fluidos en los sistemas volcánicos. Observamos una señal semejante a un tremor no armónico durante 2019 en el volcán Taupō. El análisis sísmico detallado en el dominio de tiempo y frecuencia en el lago y datos climáticos revelaron que las señales no eran de origen magmático, pero probablemente provenían de microsismos lacustres causados por condiciones especiales del viento, que generan oleaje en el lago. El rango de frecuencia de los microsismos del lago en Taupō comienza y termina con una frecuencia dominante de 0,7 a 1,0 Hz, y durante el pico de energía máxima, la frecuencia dominante es de 0,50 a 0,56 Hz. Tales señales pueden ser comunes en los lagos caldéricos y deben entenderse para que puedan distinguirse del tremor causado por la actividad volcánica para que la probabilidad de erupciones no se sobreestime.

Keywords: Volcanic lakes; Non harmonic tremor; Lake microseisms; Taupo volcano.

Submitted: 2023-05-20 | Accepted: 2024-07-03 | Published: 2024-10-22

Editor: C Caudron | Typesetter: J Farquharson

1 Introduction

Taupō volcano, part of the central Taupō Volcanic Zone (TVZ) in the North Island of New Zealand, is recognised as one of the world's most productive areas for silicic magma in the Quaternary [Wilson and Rowland 2016]. This volcano is one of two active calderas in the TVZ; [Wilson 1993], and has been active since 300 ka (Wilson and Charlier [2009]; Figure 1). On top of Taupō volcano lies Lake Taupō with an area of 622 km^2 and a maximum depth of 165 m [Gilmour 1991]. Rapid accumulation of magma and abnormally fast separation of the melt-dominant bodies in the TVZ have been attributed to the magmatic and tectonic rift setting [Wilson and Charlier 2009; Barker et al. 2014]. The youngest caldera-forming event at Taupō, the Oruanui eruption, occurred 25.5 ka ago and evacuated ~530 km^3 of magma [Wilson et al. 2006]. Reconstructions of Oruanui and post-Oruanui eruptions exhibit fast (thousands of years) regeneration and evacuation of Taupō's magmatic system [Wilson and Charlier 2009; Barker et al. 2014]. Explosive activity is frequent in the late Quaternary, and more evident in the Holocene, with 28 eruptions recognised since the Oruanui eruption [Wilson 1993].

Recent unrest periods at Taupō volcano have been observed, with approximately 22 unrest events in the past 141 years, of which five were classified as moderate [Potter et al. 2015; Illsley-Kemp et al. 2021], including the most recent periods in 2019 and 2022. These unrest periods are signified by earthquake swarms, ground deformation, hydrothermal explosions, degassing, and changes in the geothermal system [Potter et al. 2015; Illsley-Kemp et al. 2021; GeoNet 2022b]. A recent unrest period started in October 2018 and ended in September 2019 with signs of crustal deformation and seismicity. It was classified as moderate in the Volcanic Unrest Index for Taupō volcano (VUI) [Potter et al. 2015; Illsley-Kemp et al. 2021]. Another unrest episode began again in May 2022, evidenced by an elevated earthquake activity and ground deformation, which increased the Volcanic Alert Level to 1 in September 2022 [GeoNet 2022a; b] and was lowered again in May 2023 [GeoNet 2023]. Unrest at active volcanoes is often associated with a wide range of seismic signals related with fluid interaction [e.g. Konstantinou and Schlindwein 2003; Mc-

* henriette.bakkar.hindeleh@una.cr

Nutt 2005; Montegrossi et al. 2019], amongst them volcanic tremor, but these have not previously been observed at Taupō.

Several classifications for volcanic earthquakes have been proposed [e.g. Minakami 1974; Latter 1981; Ibáñez and Carmona 2000; McNutt 2005]. In general, these authors all agree that there are four types of volcanic events that are defined by their time and frequency characteristics. These are volcano-tectonic (VT) events, low frequency or long period (LP) events, volcanic tremors, and signals associated with eruptions and explosions. Volcanic tremor is denoted as a continuous seismic signal of long duration compared with earthquakes, in which vibrations lasts from minutes to days [McNutt 2005]. Variations in frequency and time of volcanic tremor cause a diversity of volcanic tremor types. Examples of this are: harmonic tremors, characterised by spectrum peaks in a narrow frequency band with overtones in a range of 0.1–12 Hz [Konstantinou and Schlindwein 2003; McNutt 2005; Montegrossi et al. 2019]; monochromatic tremor, related to a continuous signal with a unique spectrum peak in a narrow frequency band; and non-harmonic tremor referring to a continuous signal with variations in amplitude in a wide frequency band without a defined spectral peak [Mori et al. 1989; Zobin 2011].

However, the existence of a large water-body on top of a volcano may make the interpretation of these signals difficult, as more sources of background seismic noise are available within the lake which can be masked with volcanic tremor [Subira et al. 2023]. These sources are related to anthropogenic activities (boats, water pipes) and the interactions between the lake, the atmosphere, and the solid Earth [Gualtieri et al. 2014]. Wind-generated seismic noise has been identified at frequencies ≥2 Hz; these effects are due to interaction with ground, trees, or water bodies [Smith and Tape 2019]. In addition, the high attenuation across the region can cause volcano-tectonic events (VT) to be mistaken for low frequency seismic signals (LP), as demonstrated by Illsley-Kemp et al. [2022].

Low frequency seismic oscillations have been identified in large lakes as the Great Slave Lake, Lake Ontario, the Great Lakes, and Yellowstone Lake in North America, the Fuxian Lake, Erhai Lake in China, and the Lake Malawi in Africa [Xu et al. 2017; Anthony et al. 2018; Smalls et al. 2019; Farrell et al. 2023] caused by the interaction of the atmosphere, the lake, and the bottom of the lake. These microseisms have been identified as lake-generated microseisms and are analogous to the ocean microseisms in terms of generation. The period of sustained seismic signals at lakes are distinct in comparison with the ocean microseisms, which range between 0.5–2 s [Xu et al. 2017; Anthony et al. 2018; Smalls et al. 2019] for the lake microseisms and 2–20 s for the ocean microseisms [Longuet-Higgins 1950; Hasselmann 1963; Ardhuin et al. 2011].

Two mechanisms have been proposed as the cause of a sustained seismic signal [Longuet-Higgins 1950; Hasselmann 1963; Ardhuin et al. 2011] for ocean microseisms: a linear and non-linear interaction of water waves with the solid Earth, and with opposite waves' direction, respectively. Both interactions produce changes in pressure at the bottom of the ocean that causes the continuous oscillation of the ground. Two main peaks are associated with the primary and secondary ocean microseisms. The primary microseisms are caused by the interaction between water gravity waves and the bathymetry in shallow water. The dominant seismic peak of the primary microseisms have the same period as the water gravity waves in shallow depths [Longuet-Higgins 1950; Hasselmann 1963]. The secondary microseisms have higher energy content and half the period compared to the primary microseisms. This seismic signal is generated by the interaction of two gravity waves travelling in opposite directions [Longuet-Higgins 1950; Ardhuin et al. 2011].

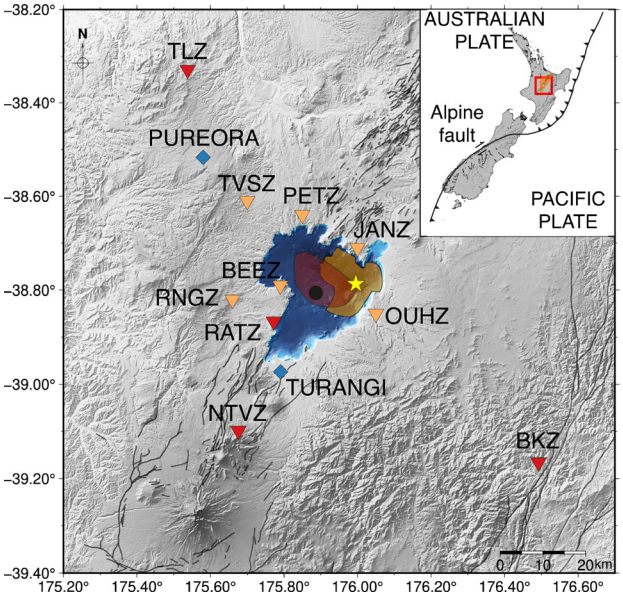

Figure 1: A summary map of the tectonic and volcanic features at Taupō volcano. The inset figure shows the Australian and Pacific Plate boundary [black lines; Coffin et al. 1997], the TVZ (orange area) and the study region (red box). Oruanui and Taupō structural calderas are shown in red and orange areas respectively. The most recent volcanic vent is represented with a yellow star [Barker et al. 2021], and the active faults in the region with grey lines [Langridge et al. 2016]. Locations of seismic stations from GeoNet are shown with red and from ECLIPSE with orange inverse triangles. Blue diamonds correspond to NIWA weather stations. The black filled circle marks the reference point of the centre of Lake Taupō.

While the generation mechanism of primary and secondary lake microseisms bears resemblance to the ocean microseisms, the first one shows fluctuations in amplitude and frequency. This variability is influenced by the interaction of factors such as wind, bathymetry, shoreline characteristics, and the lake's fetch in a local closed system [Carchedi et al. 2022; Farrell et al. 2023].

Ciacy [1973] recognised a transient seismic noise during a seismic deployment in the north shore of Lake Taupō during 1966, and related this seismic signal with frequencies from 0.1–15 Hz to wind storms, identifying this noise as lake microseisms. Based on one month of data (25 February to 19 March 1966) Ciacy [1973] observed a minimum duration of one hour and a maximum duration of 18 hours of the lake microseisms.

Low frequency seismic energy (0.5–3 Hz) in active volcanic contexts can be affected by other seismic noises, as has been recently identified in Nyiragongo and Nyamulagira volcanoes, in Democratic Republic of the Congo [Subira et al. 2023]. Seasonal and diurnal lake microseisms with a frequency range of 0.4–2 Hz strongly influenced the seismic energy at nearby stations of Lake Kivu.

In this paper, we describe a non-harmonic-like tremor signal at Taupō associated with lake microseisms using the continuous monitoring records from 2019. In a volcanic environment, especially during an unrest period, understanding the origin of the seismic signals provides a clue to the volcano dynamic in terms of preparedness and response.

2 Data and methods

2.1 Seismic analysis

We reviewed the continuous seismic data (waveforms, spectra, and spectrograms) using the vertical component of the GeoNet broadband seismic station RATZ (Figure 1) to create a catalogue of volcanic, anthropogenic or instrument-related seismic noises or signals at Taupō volcano. A fully manual review of the continuous stream was done for 2019 using the SWARM software [Norgaard et al. 2021] for visualisation in time and frequency domains (Figure A1). The selection of RATZ as the reference station relates to its proximity to the recent volcanic vents of Taupō, and it was the only broadband station of the GeoNet network near Taupō volcano during 2018–2019 (Figure 1). Finally, because it is located away from roads and Taupō town, relatively free of anthropogenic noise in the frequency band of interest.

Within the seismic signals in the preliminary catalogue, we recognised high frequency events and low frequency tremor-like signals. To further comprehend the origin of these signals, we compared observations from the reference station with those from broadband stations within a radius of 50 km from Lake Taupō. We selected GeoNet stations for the temporal range of 2019 (TLZ, BKZ, and NTVZ) and selected stations from the temporary ECLIPSE seismometer network [Mestel et al. 2019] (PETZ, BEEZ, OUHZ, JANZ, RNGZ, and TVSZ) for December 2019 (Figure 1). The sampling rate of the continuous seismic data was 100 Hz. We also calculated the seismic energy in the low frequency range (0.4–6 Hz) during December 2019 by the Real-Time Seismic Energy Measurement [De la Cruz-Reyna and Reyes-Dávila 2001] for the stations mentioned above (Figure 2).

In order to verify the single-station detection of lake microseisms at RATZ, we also studied the spatial coherence of the seismic wavefield, using streams of continuous vertical components from seismic stations around Lake Taupō. To do so, we used the software CovSeisNet for the detection of coherent signals across the network [Soubestre et al. 2018]. This method estimates the eigenvalues of a seismic network covariance matrix to identify the coherence in the frequency domain of the seismic network. A single localised seismic source will be represented with a low spectral width that is coherent in the seismic network, whereas a distributed ambient seismic noise will be represented with a high spectral width [Soubestre et al. 2018].

From time-frequency analysis at RATZ and the temporary ECLIPSE network, we observed a seismic noise with frequencies up to 45 Hz (Figure 3) that persisted for minutes to days coincident with the occurrence of a low frequency seismic signal in the range of 0.4 to 6 Hz (Figure A1). To determine the start and the end of these lake microseism signals, we observed that the dominant spectral peak was usually 0.4–1.0 Hz; see also Sections 3.1 and 4.1. However, during the occurrence of the lake microseisms the dominant spectral peak decreased to 0.4–0.5 Hz (Figures 4 and A1). A catalogue of the details of lake microseisms is provided in Table A1 in Appendix A.

To determine the ambient seismic noise at Lake Taupō we calculated the probabilistic power spectral density (PPSD) for the continuous data using the McNamara and Buland [2004] method. For this calculation we used hourly traces of the vertical channel of RATZ station, with an overlap of 50 % from the period January 2019–December 2019 (Figure 6).

Complementary parameters such as local earthquake magnitudes are considered in the time series analysis to determine the possible source of the low frequency tremor-like signals (Figure 5).

2.2 Weather data analysis

To determine or discard a relation between the continuous seismic analysis and climatological factors, we compared low frequency seismic energy (0.4–6 Hz) to surface wind speed, wind orientation and maximum wind gust speed in hourly measurements from the Tūrangi and Pureora National Institute of Water and Atmospheric Research (NIWA) weather stations (Figures 1 and 5). We searched for times in which the wind direction was consistent for a minimum of three hours and had a circular standard deviation of 10° from Tūrangi surface wind data (Figure 6). Afterwards, we compared mean wind speed, mean wind orientation and duration of the consistent wind periods with the low frequency seismic energy in 2019.

3 Results

3.1 Lake microseisms at Taupō volcano

We identified lake microseisms at Lake Taupō as low frequency continuous seismic oscillations with frequencies between 0.4 and 1.0 Hz (Figure 3). During the maximum peaks of seismic energy, the dominant frequency content of lake microseisms is in the range 0.50–0.56 Hz, however this particular signal in Taupō starts and ends with a dominant frequency in the range 0.7–1.0 Hz (Figure 3 and A1). This signal is registered at broadband seismic stations as far as 27 km from the centre of Lake Taupō (Figures 1 and 2). Lake microseisms are observed during all months of 2019 and recognised in six temporary broadband stations surrounding the lake (BEEZ, PETZ, JANZ, OUHZ, RNGZ, TSVZ) and seven permanent seismic stations. During 2019, the duration of lake microseisms ranged from hours (4 h) to days (68 h) (Table A1).

Lake microseisms contain frequencies up to 3 Hz generally (Figures 3 and 7), however exceptional cases reach up

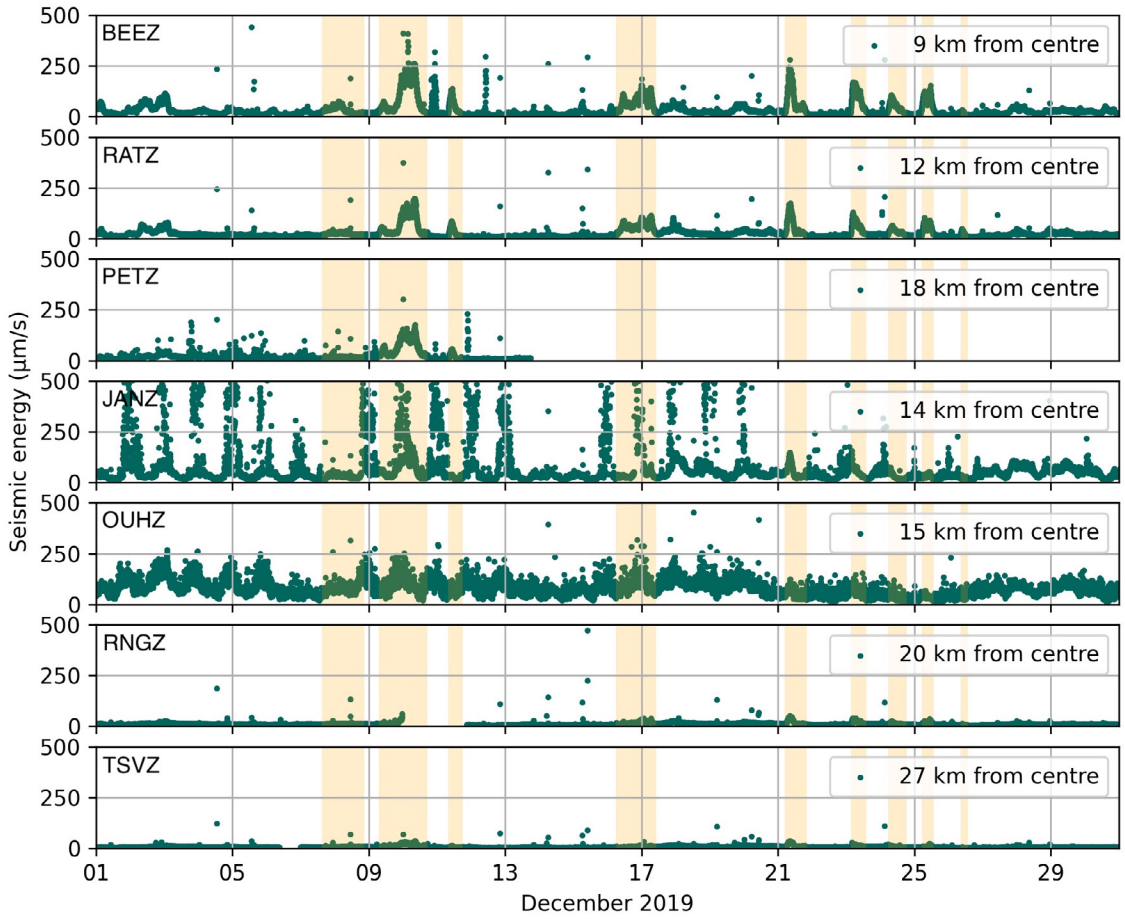

Figure 2: Seismic energy plots at seven broadband stations (Figure 1) around Taupō during December 2019. The vertical continuous stream of each station is filtered between 0.4 Hz and 6.0 Hz. Each subplot is ordered from higher (top) to lower (bottom) seismic energy content considering the maximum values of the low frequency signal. The orange areas show the occurrence of lake microseisms and values in the upper right indicate distance from the centre of Lake Taupō. PETZ station was not functional after December 14, and RNGZ station was not functional from December 10 to December 12.

to 6 Hz. The spectrogram of intense lake microseisms (up to 6 Hz; Figure 7) at Lake Taupō is similar to non-harmonic tremors registered at active volcanoes with hydrothermal systems [Dmitrieva et al. 2013; Hall et al. 2013; van der Laat et al. 2022].

We calculated the probabilistic power spectral density [PPSD; McNamara and Buland 2004] of the RATZ vertical channel continuous traces during 2019 in two types of periods: 1) excluding the temporal occurrence of lake microseisms and 2) only including the temporal occurrence of lake microseisms. From these, we identified a dominant frequency peak associated with lake microseisms at 0.50–0.56 Hz as shown in Figure 4. This peak does not appear when we exclude the traces with the occurrence of lake microseisms in the PPSD calculations, based on Table A1.

The coherence of the lake microseism across GeoNet stations and ECLIPSE stations is concordant with our observations at RATZ seismic station. Lower spectral width indicates a higher coherence of a single source in the network. We observed a higher frequency at the beginning and end of the lake microseism (0.7–1 Hz), and a decrease of the dominant frequency during the lake microseism (0.50–0.56 Hz) with low spectral width values, as exemplified in Figures 3 and 8. Prior to the start of the lake microseism, we recognised a coherence in the network from 0.1–0.5 Hz that prevails during the lake microseism (Figure 8).

4 Discussion

4.1 What causes lake microseisms at Taupō volcano?

Wind and rain data from two weather stations were analysed and compared with the seismic energy data to identify any correlation. We selected hourly data from NIWA weather stations located at Tūrangi and Pureora (Figures 1, 5, A2, and A3).

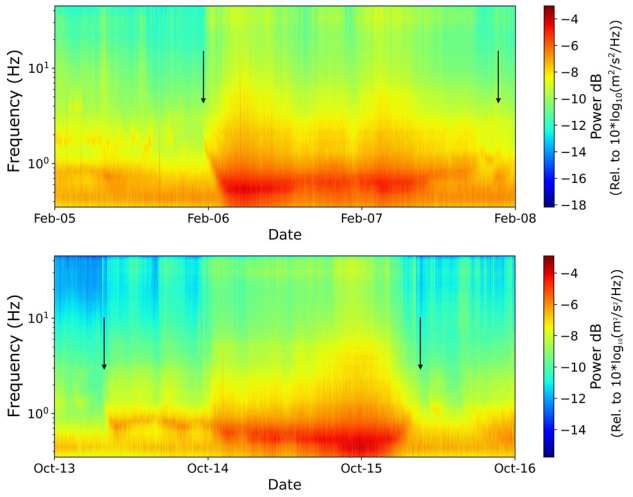

Figure 3: Spectrogram of lake microseisms during 6–7 February (top) and October 13–15, 2019 (bottom) from RATZ station using Obspy [Beyreuther et al. 2010]. The window length of the STFT used was 1024 samples. The black arrow shows the start and end of the lake microseisms.

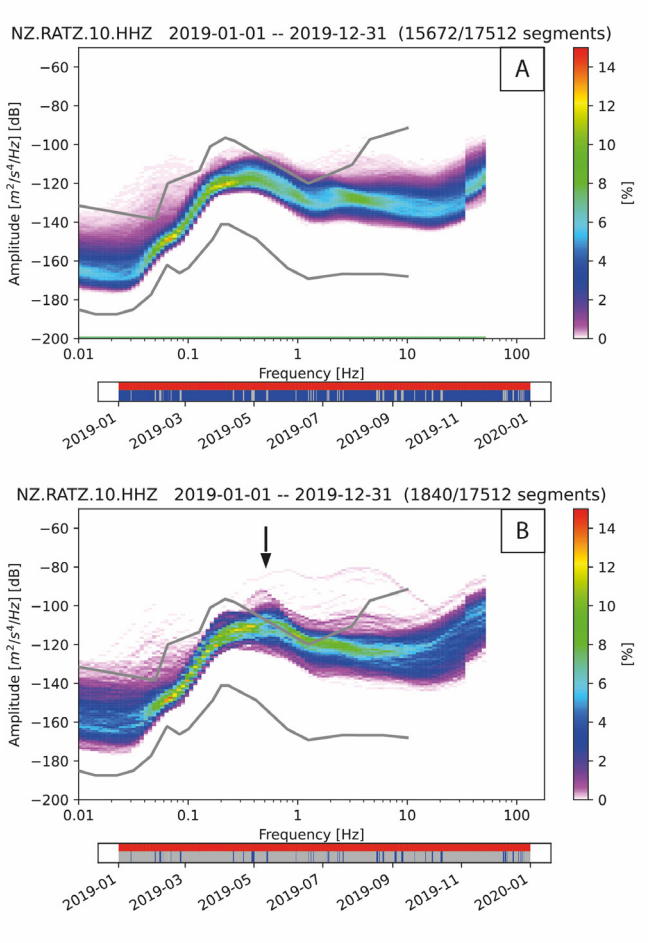

Figure 4: Probability density function for ambient seismic noise recorded with the vertical channel of RATZ seismic station using Obspy [McNamara and Buland 2004; Beyreuther et al. 2010]. The grey lines indicates the low and high noise models by Peterson [1993]. [A] Excluding traces with the occurrence of lake microseisms during 2019 based on Table A1. [B] Using traces with the occurrence of lake microseisms during 2019 based on Table A1. The black arrow indicates the dominant frequency related to lake microseisms at Taupō volcano.

At Tūrangi (near Lake Taupō), surface wind and maximum wind gust preferentially arrive from the SW and SE, however northern surface winds are recorded (Figure A2). At Pureora Forest Park surface wind and maximum wind gust mainly arrive from N–NW and S–SE (Figure A2). Yet, periodicity of higher wind speeds are identified during the daytime in both stations. Mean wind speed during the period 2018–2019 tended to be higher during August–December. The monthly total precipitation was higher during winter (June–August), with the exceptions of December and April, which were also high (Figure A3). We used the Pearson correlation coefficient to measure the linear correlation between two variables. This method uses the ratio between the covariance of two variables and product of their standard deviations [Pearson 1895]. The estimated Pearson correlation between low frequency seismic signals and rain for three-minute sampled data is 0.028, which indicates no relationship between these two variables.

We recognised a pattern of consistent wind orientation that prevails for more than three hours prior to the occurrence of lake microseisms in 2019; in some cases prior to and during the occurrence of a lake microseism as represented in Figure 6. The minimum wind speed to have these conditions on Lake Taupō is 6 km h^{-1}, however the mean wind speed is 13 km h^{-1} based on 2019 analysis. With a larger dataset, this condition could vary. We observed a major coincidence in the occurrence of lake microseisms with NW–SE orientations of consistent wind as indicated in Figures 6 and 9.

Similarly to wind-driven waves in the ocean, we propose that the consistent wind at Lake Taupō creates similar conditions and generates the lake microseisms at the bottom of the lake. We observed a correlation between higher consistent wind speeds and the seismic energy (Figures 6 and 9). Correspondingly, we observed higher values of seismic energy from longer periods of consistent wind direction at Lake Taupō (Figures 6 and 9).

Consistent wind orientations at 330–350° (NW) and 130–180° (SE) are the most frequent orientation prior to or during the occurrence of a lake microseism as observed in August 17 and 19, 2019 (Figure 6A), and during December 21, 23–26 (Figure 6C). Some of the consistent wind orientation occurred prior to the lake microseisms, and some of them during the lake microseisms. Wind speed in these cases are < 15 km h^{-1} (December 21, 23, 24, 25, and 26) and caused higher seismic energy of lake microseisms than the consistent wind oriented at 250° (December 28). Seismic energy appears to be higher when the wind speed is higher for similar consistent wind orientations as demonstrated in different lake microseisms during December, 2019 (Figure 6C) and October 13 (Figure 6B). The October 13 lake microseism represents the highest seismic energy event with preferred wind orientations coming from 120–130°, and surface wind speed greater than > 20 km h^{-1} (Figure 6B).

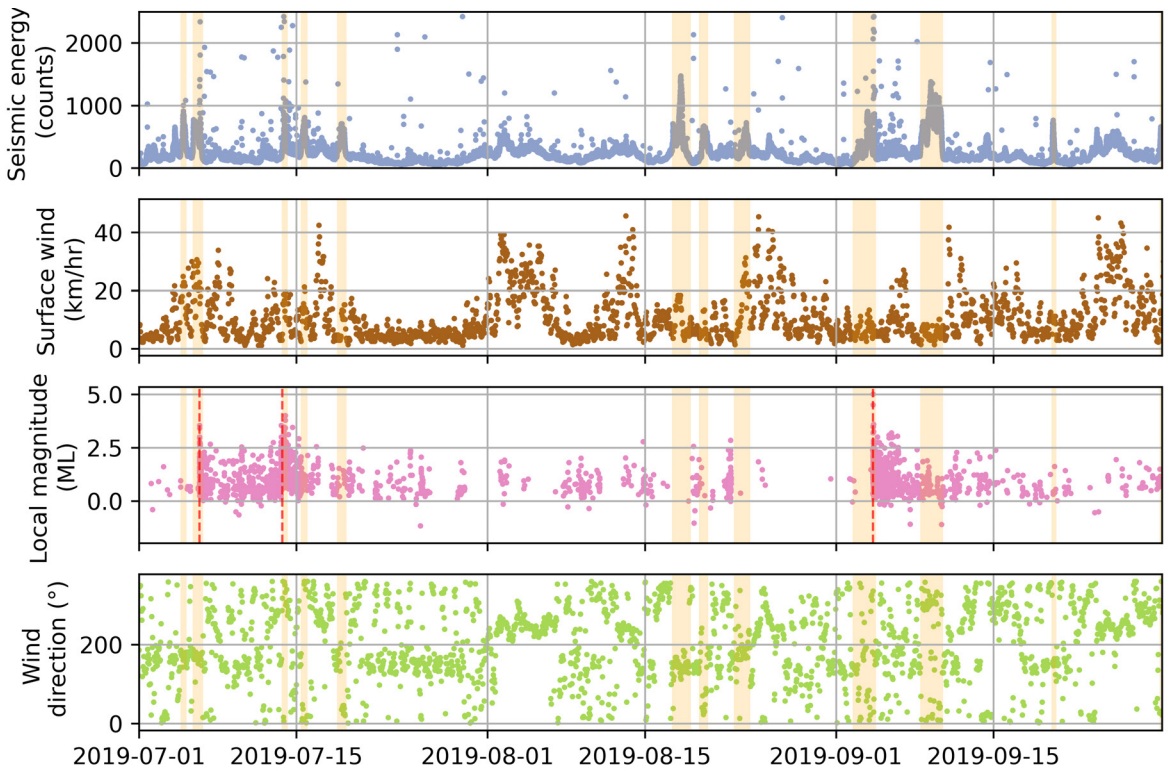

Figure 5: Time-series plots of seismic energy, wind speed, local earthquake magnitudes (from Illsley-Kemp et al. [2021]) and wind direction using seismic data from RATZ stations and weather data from Tūrangi station. Orange areas correspond to the temporal occurrence of lake microseisms (Table A1), during July–September 2019. Vertical red lines correspond to the start of earthquakes swarms during July–September 2019.

Wind direction seems to be a crucial factor in the energy and occurrence of lake microseisms. Prolonged periods of consistent wind with high wind speeds (> 25 km h^{-1}) did not cause lake microseisms, or caused very weak events, as observed during 1–5 August, 2019 (Figure 6A), when the surface wind had a consistent orientation of $\approx 250°$. Overall, consistent wind direction coming from the west and southwest of Lake Taupō did not generate evident lake microseisms (Figures 6, 9). However consistent wind from a NW or SE orientation did generate lake microseisms (Figures 6, 9).

The signal of lake microseisms starts and ends with a dominant frequency of 0.7–1.0 Hz, and during the maximum energy peak, the dominant frequency is of 0.50–0.56 Hz (Figure 3). We identify this signal in all broadband stations around the lake with a constant level of energy, dependent on the station location (Figure 2). The spectrogram during these particular signals are characterised by an increase in noise levels up to 45 Hz, likely associated with noise caused by the high wind speeds and the wind-driven waves from these higher wind speeds within the lake.

Stations closer to the centre of the lake (BEEZ and RATZ) showed higher seismic energy peaks in frequency band of 0.50–6 Hz (Figure 2). This supports our assertion that the source for the low-frequency microseism is within the lake.

4.2 How does wind generate a low-frequency microseism?

The presence of a large water-body, anthropogenic activity, an active volcano, and varying weather conditions all contribute to a range of seismic noise at Taupō. We recognised a particular signal that has similarities to a volcanic seismic signal during 2019: the lake microseism (Figure 8). Time-frequency analysis of 2019 data using RATZ station and the ECLIPSE temporary network plus weather data provided evidence that the low frequency seismic signals identified at Taupō are not related to a volcanic source, but are caused by sustained wind.

Studies have shown low frequency signals known as lake microseisms at seismic stations near large lakes such as Ontario Lake [Kerman and Mereu 1993], Yellowstone Lake [Smalls et al. 2019; Farrell et al. 2023], Lake Malawi [Carchedi et al. 2022], the Great Slave Lake, Dianchi Lake, Fuxian Lake, and Erhai Lake [Xu et al. 2017]. In general, the authors identify peaks of seismic energy at a dominant frequency of 0.5–2 Hz associated with lake microseisms observed in lakes with areas between 210 km^2 and 27,000 km^2 [Xu et al. 2017]. In a volcanic settings, lake microseisms can be masked within the volcanic tremor from nearby sources as previously identified in the Virunga Volcanic Province [Subira et al. 2023]. With an area of 622 km^2 at Lake Taupō, we observed a similar pattern with a dominant frequency peak of 0.50–0.56 Hz (Figure 4).

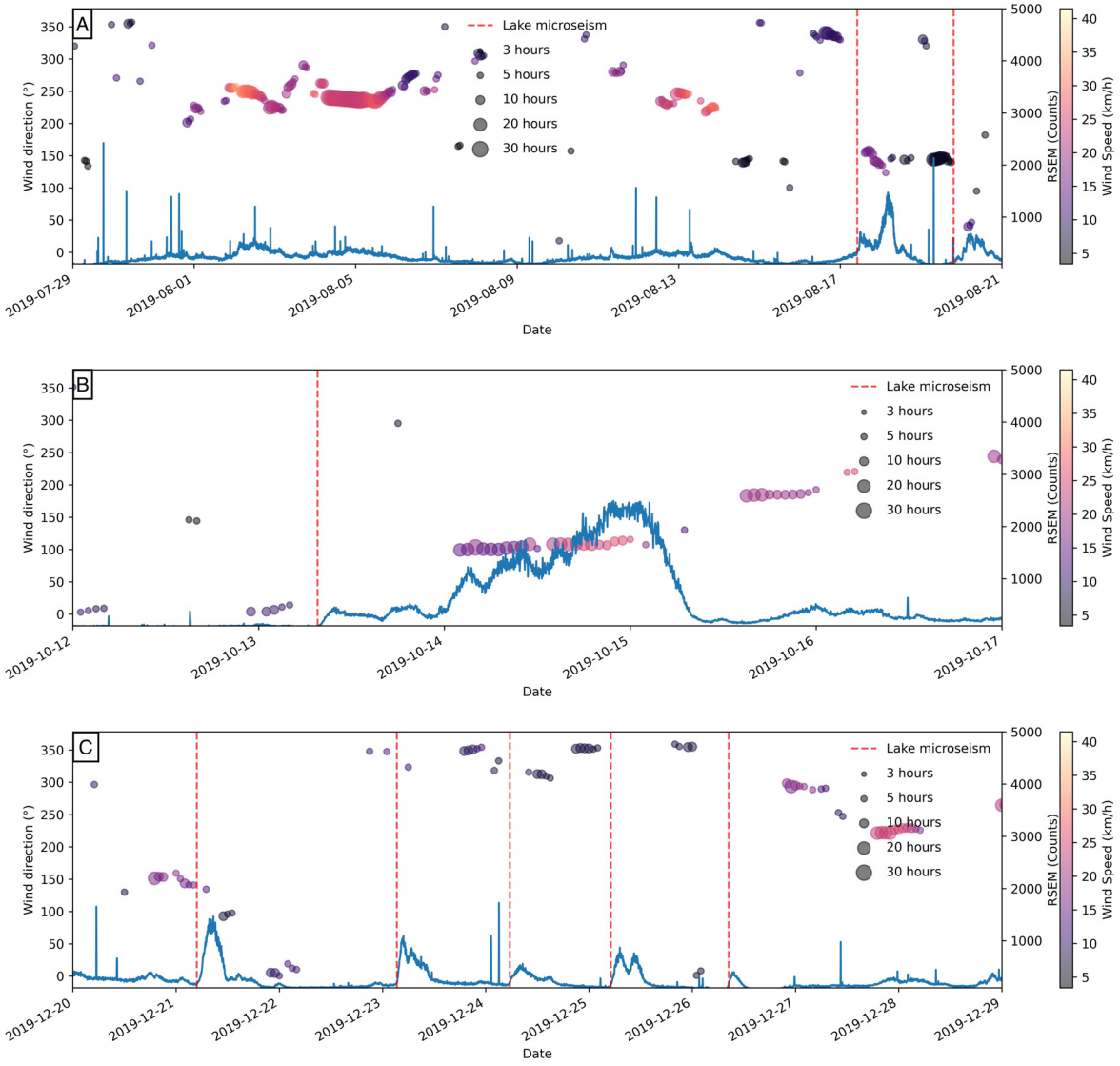

Figure 6: Comparison between seismic energy using the RATZ seisimic station and wind data from Tūrangi weather station. The circles indicates time periods in which the surface wind was consistent in direction for more than 3 hours. The colour of the circles shows the wind speed, and the sizes the duration of the sustained wind. The blue line shows the seismic energy. The left y-axis indicates the mean orientation of the wind, whereas the right y-axis shows the seismic energy in counts. Vertical red lines correspond with the start of lake microseisms. Panel [A] exemplifies a case in which consistent wind orientation at ≈250° for ≈ 40 hours did not cause a lake microseism during 1–5 August with wind speeds > 25 km h^{-1}. Panel [B] illustrates the lake microseisms with the highest seismic energy during October 14, 2019 in which the consistent wind orientation was ≈25° prior to and 130° during the lake microseisms. Panel [C] shows the occurrence of five lake microseisms during December 2019 in which the consistent wind orientation was NW (300–350°) and SE (150°).

In general, these low frequency continuous seismic oscillations can be registered by seismic stations within 25–30 km [Xu et al. 2017] with higher seismic amplitudes closer to the bottom of the lake. Yet, few studies mention the existence of lake microseisms in a volcanic setting, as in the case of Yellowstone [Xu et al. 2017; Smalls et al. 2019; Farrell et al. 2023] and Taupō in this study.

At Lake Taupō, lake microseisms commence and conclude with higher frequencies ranging from 0.7 to 1.0 Hz, and during the maximum energy peak, the dominant frequency is of 0.50–0.56 Hz as evidenced in Figures 7 and 4. On a broader scale, the probabilistic power spectral density analysis (Figure 4) did not reveal an additional peak occurring between 0.7 and 1.0 Hz. Carchedi et al. [2022] recognised two peaks attributed to primary and secondary lake-generated microseisms. Farrell et al. [2023] provided evidence of double frequency microseism with dominant frequencies of ~0.8–1.2 s from wind, wave gauges, and lake bottom seismometers observations at Yellowstone Lake. Yet, the mechanisms of primary and secondary microseisms are not from a unique source, but complex and influenced by the shoreline, bathymetry and wind-wave interactions [Carchedi et al. 2022; Farrell et al. 2023].

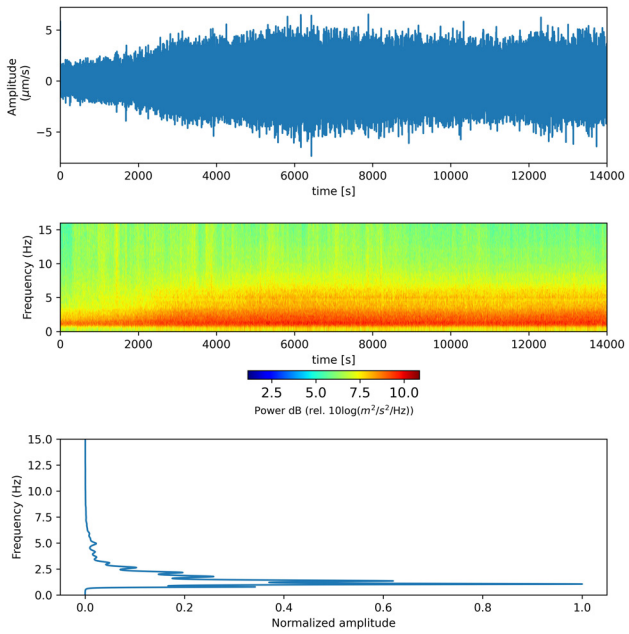

Figure 7: Waveform (upper), spectrum (lower) and spectrogram (middle) of a lake microseism during April 21, 2019 08:00 UTC. We applied a high-pass filter of 1.0 Hz using Obspy [Beyreuther et al. 2010] and calculated the spectrogram with the Short Time Fourier Transform [Marple Jr and Carey 1989]. The window length of the STFT used was 512 samples.

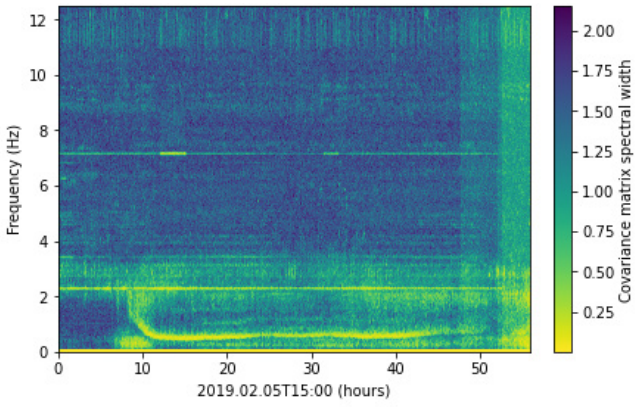

Figure 8: Covariance matrix spectral width during 6–7 February, 2019 with GeoNet stations around Taupō with an overlapping window of 30-seconds using CovSeisNet [Soubestre et al. 2018]. The low values of the spectral width confirms a single localised source (lake microseism) coherent in the seismic network.

The Rayleigh-Rg wave is the most common type of wave observed in lake microseisms [Kerman and Mereu 1993; Xu et al. 2017; Anthony et al. 2018]. Periodicity in the occurrence of lake microseisms has been identified in several studies related to daily and seasonal variations of wind speed or frozen conditions of the lake, as observed in Yellowstone [Smalls et al. 2019; Farrell et al. 2023], Lake Malawi [Carchedi et al. 2022] and Yunnan Lake [Xu et al. 2017]. Non-periodic lake microseisms have also been identified in Lake Ontario, associated with the passage of storms at the lake [Kerman and Mereu 1993; Kerman et al. 1995]. A recent study using lake-bottom seismometers, land-based seismometers, weather stations, and wave gauges identified diurnal lake microseisms at Lake Yellowstone [Farrell et al. 2023]. These lake microseisms with dominant frequencies of ~0.8–1.2 s were caused by the interaction of the incident waves with the shoreline–reflected waves, analogous to secondary microseisms [Farrell et al. 2023].

The lake microseisms we identify at Lake Taupō have dominant frequency oscillations between 0.4–1.0 Hz. During consistent wind direction (± 10°) and high wind speed (>15 km h^{-1}), from a NW or SE direction, we observed a continuous seismic noise that reached frequencies up to 6 Hz, e.g. during April 21, 2019 (Figure 7). In these conditions, lake microseisms have similar characteristics to non-harmonic tremors in volcanic areas, as observed in (among others) Ruapehu, Whakaari, and Turrialba volcanoes [Dmitrieva et al. 2013; Hall et al. 2013; van der Laat et al. 2022]. During 2019, we identified 38 lake microseisms associated with sustained wind (Table A1 and Figure A1) with a minimum duration of 4 hours and a maximum of 68 hours. Ciacy [1973] previously observed a similar signal at Taupō.

Orientation of the consistent wind clearly influences the generation of lake microseisms. We identified high wind speeds and extended hours of consistent wind that did not cause lake microseisms (Figure 6A). We attribute this condition to a shorter fetch distance of winds coming from the W and SW. In contrast, higher seismic energy is attributed to wind coming from N–NW and S–SE. In this orientation, the northern section of the lake has its maximum fetch (Figure 1), and a greater water depth and sediment thickness due to caldera collapse [Davy 1993].

Even though the seismic signals generated at Taupō are caused by the interactions between the lake and specific weather parameters, we found similarities between their seismic signals and non-harmonic volcanic tremor. The evaluation of low frequency seismic energy in ECLIPSE stations around Lake Taupō supports the idea that it is not a local source from the observation station, but a local source within the lake. Seismic peaks were identified in stations between 10 and 28 km from the centre of the lake, dissipating outwards from the lake (Figure 2). These lake microseisms are a local source of ambient noise (surface waves) and could be useful for imaging shallow crustal structures at Taupō, as proposed from worldwide studies of lake microseisms [Xu et al. 2017].

Lake microseisms are commonly observed in large lakes, however, in water-filled calderas, such reports are rare. Yellowstone [Xu et al. 2017; Smalls et al. 2019] and Taupō volcano (this study), are exceptional cases of the occurrence of lake microseisms in a water-body on top of a volcano. However, in Taupō the water-body covers the caldera completely, while in Yellowstone, the caldera is only partially covered. Recognising seismic signals in a volcano with an eruptive potential such as that of Taupō is of great importance. Prior studies of volcanoes often use volcano seismology and time-frequency analysis to monitor the evolution of the magmatic system and as a tool for forecasting eruptions in active and dormant volcanoes [e.g. Gómez M and Torres C 1997; Nabyl et al. 1997; Green and

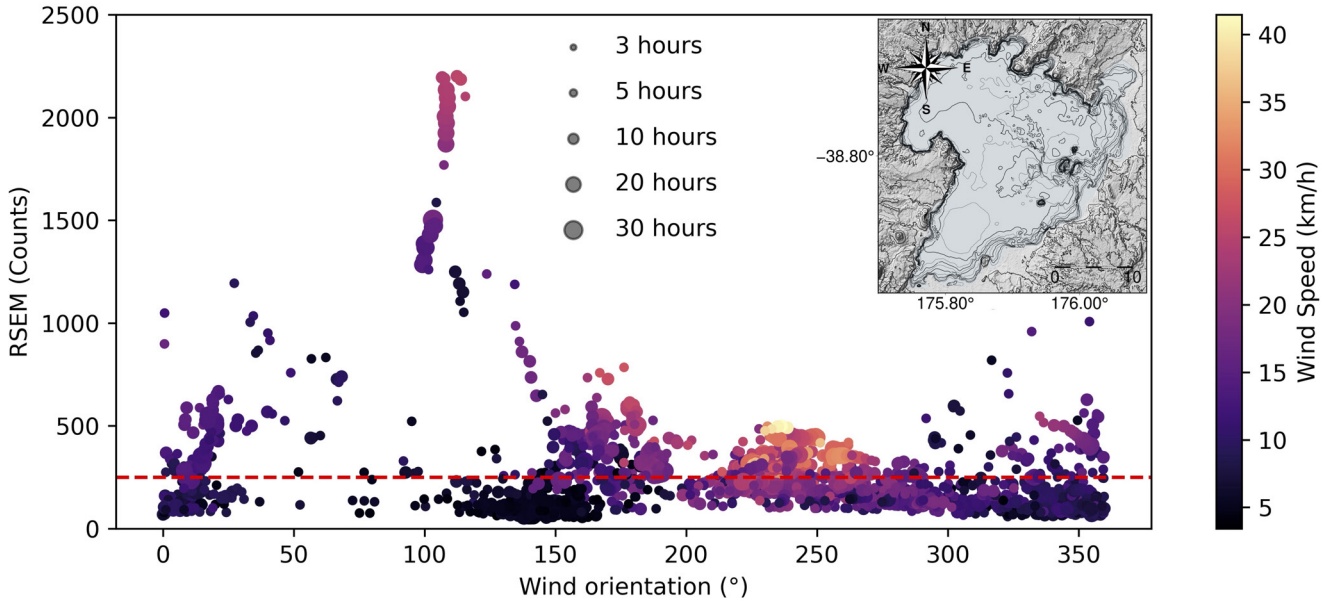

Figure 9: Relation between circular mean wind orientation and seismic energy during times in which the wind was consistent for more than 3 hours and with a standard deviation of ±10°. The exceptional seismic energy points (> 1400 counts) are related to the October 13 lake microseism. The most frequent periods of elevated seismic energy occur when the wind orientation is between 0–25° (NE), 330–360° (NW) and 130–180° (SE). In the upper right corner is a map of Lake Taupō with elevation contours, including the lake bathymetry. The red dashed line indicates the RSEM value at which lake microseisms were identified during 2019.

Neuberg 2006; Lesage et al. 2006]. On the other hand, misinterpreting lake microseisms as volcanic tremor may cause confusion in the alert level systems, and therefore may activate false volcanic responses. Our findings are an important consideration for future monitoring of Taupō, or indeed any volcano with a major lake.

4.3 Lake microseisms as a trigger of earthquake swarms?

Lake microseisms have been identified in large lakes around the world, with frequency contents in a range of 0.5–2.0 Hz, and often polarised as Rayleigh waves [Xu et al. 2017]. These seismic signals can be periodic and related to daily variations in wind velocity due to changes in temperatures, or related to storms and the interaction of two waves travelling in opposite directions [e.g. Kerman et al. 1995; Xu et al. 2017; Smalls et al. 2019].

If we consider the passage of surface waves through a magmatic reservoir with frequency content similar to the lake microseisms, we could consider the possibility that the lake microseisms could alter the stress condition of the hydrothermal-magmatic system. Moreover, these lake microseisms are a local and sustained source of surface waves above the volcano, and should be studied in more detail to fully understand their relationship to the volcano. Surface waves travelling through active volcanoes have been identified as a possible trigger of eruptions or seismic swarms within their systems, e.g. Puyehue–Cordón Caulle in 1960 after a 9.5 M_W earthquake [Lara et al. 2004], Hakone volcano, in Japan, recorded triggered seismicity after the passage of surface waves from the Tōhoku–Oki 9.1 M_W earthquake [Yukutake et al. 2013], and Villarica volcano in 1730, 1737, 1822, 1837, and 1930 had eruptions shortly after the occurrence of large earthquakes (≥7.5 M_W) [Linde and Sacks 1998; Watt et al. 2009]. The passage of surface waves from distant earthquakes through magmatic and hydrothermal systems are considered to trigger seismic swarms and volcanic eruptions by oscillations of the dynamic stresses [Seropian et al. 2021]. Yet, seismicity at hydrothermal systems is triggered with smaller dynamic stresses than at magmatic systems [Seropian et al. 2021]. We identified lake microseisms that occurred prior to or during an earthquake swarm (RSEM in Figure 5). During the unrest period, nine of the 38 recognised lake microseisms occurred prior to or during an earthquake swarm; e.g. July 6, July 13, and September 4 (Figure 5). Most of the lake microseisms that occurred prior to or during the earthquakes swarms happened during June–September (Figure 5), which has been specifically associated with magmatic intrusion [Illsley-Kemp et al. 2021]. We suggest that in certain critical stress conditions such as in 2019, lake microseisms may trigger earthquakes at Taupō. However, lake microseisms also occur during time periods without any evident relation with earthquakes. Thus, more extensive studies of Taupō are necessary to identify any relationship between lake microseisms and earthquakes.

5 Conclusions

In summary:

- We recognised a particular signal that has similarities to a volcanic seismic signal during 2019: the lake microseism.

• Lake microseisms have oscillations between 0.4–1.0 Hz, with a dominant frequency peak of 0.50–0.56 Hz. During intense and sustained wind conditions with preferential orientations, we observed a continuous seismic noise that reached frequencies up to 6 Hz. In these conditions, lake microseisms have similar characteristics to non-harmonic tremors in volcanic areas, as observed in Ruapehu, Whakaari, and Turrialba volcanoes [Dmitrieva et al. 2013; Hall et al. 2013; van der Laat et al. 2022].

• During 2019, we identified 38 lake microseisms associated with consistent wind direction (±10°) for extended hours (> 3 hours) prior to the occurrence of a lake microseism; in some cases prior to and during the event. We observed a correlation between wind speed and the duration of the consistent wind with the seismic energy, depending on the wind orientation.

• Even though the seismic signals generated at Taupō are caused by the interactions between the lake and specific weather parameters, we found similarities between their seismic signals and non-harmonic volcanic tremor. Therefore, future monitoring of Taupō must carefully consider the interpretation of tremor-like signals.

Author Contributions

Henriette Bakkar: Processing, investigation, writing the draft, figures. **Martha Savage:** Supervision, revision of the draft and feedback. **Finnigan Illsley-Kemp:** Supervision, revision of the draft and feedback. **Eleanor Mestel:** Revision of the draft and feedback. Sharing the ECLIPSE data and the valuable discussions and the figure of PPSD.

Acknowledgements

The Ministry of Foreign Affairs and Trade of the New Zealand Government provided the Manaaki New Zealand Scholarship to Bakkar. Mestel, Illsley-Kemp and Savage were funded by the ECLIPSE programme, which was funded by the New Zealand Ministry of Business, Innovation and Employment (MBIE). Illsley-Kemp was also funded by the Toka Tū Ake EQC Programme in Earthquake Seismology and Tectonic Geodesy at Victoria University of Wellington and the Marsden Fund of the Royal Society of New Zealand (VUW2109 and UOA2220). The seismic data from the ECLIPSE network instruments was recorded across the Taupō region at sites within the rohe of Ngāti Tūwharetoa (including Ngāti Haa, Ngāti Hine, Ngāti Moekino, Ngāti Rauhoto, Ngāti Rongomai, Ngāti Ruingarangi, Ngāti Te Kohera, Ngāti Te Rangiita, Ngāti Te Urunga, Ngāti Tūrangitukua, and Te Kapa o Te Rangiita) and Ngāti Rereahu (Te Hape B and Tiroa E Trusts). We acknowledge and thank all of the individuals, communities, Iwi, Hapū, Trusts and organisations partnered with throughout the ECLIPSE programme. Javier Pachecho, Mauricio Mora and Guillermo Alvarado provided feedback. Mauricio Mora shared the MATLAB code for the calculation of the RSEM.

Data Availability

The seismic data used in this study are freely available in GeoNet (geonet.org.nz) through their public website. They are funded by the Earthquake Commission and GNS Science. The seismic data for the ECLIPSE temporary network is freely available after embargo in The IRIS Data Management Center (IRISDMC) through their public website http://service.iris.edu/fdsnws/dataselect/1/. Weather data used in this study is freely available from the National Institute of Water and Atmospheric Research (NIWA) (https://cliflo.niwa.co.nz/).

Copyright Notice

References

Anthony, R. E., A. T. Ringler, and D. C. Wilson (2018). "The widespread influence of Great Lakes microseisms across the midwestern United States revealed by the 2014 polar vortex". *Geophysical Research Letters* 45(8), pages 3436–3444. DOI: 10.1002/2017gl076690.

Ardhuin, F., E. Stutzmann, M. Schimmel, and A. Mangeney (2011). "Ocean wave sources of seismic noise". *Journal of Geophysical Research: Oceans* 116(C9). DOI: 10.1029/2011jc006952.

Barker, S. J., C. J. N. Wilson, E. G. C. Smith, B. L. A. Charlier, J. L. Wooden, J. Hiess, and T. R. Ireland (2014). "Post-supereruption magmatic reconstruction of Taupo volcano (New Zealand), as reflected in zircon ages and trace elements". *Journal of Petrology* 55(8), pages 1511–1533. DOI: 10.1093/petrology/egu032.

Barker, S. J., C. J. N. Wilson, F. Illsley-Kemp, G. S. Leonard, E. R. H. Mestel, K. Mauriohooho, and B. L. A. Charlier (2021). "Taupō: an overview of New Zealand's youngest supervolcano". *New Zealand Journal of Geology and Geophysics* 64(2-3), pages 320–346. DOI: 10.1080/00288306.2020.1792515.

Beyreuther, M., R. Barsch, L. Krischer, T. Megies, Y. Behr, and J. Wassermann (2010). "ObsPy: A Python toolbox for seismology". *Seismological Research Letters* 81(3), pages 530–533. DOI: 10.1785/gssrl.81.3.530.

Carchedi, C. J. W., J. B. Gaherty, S. C. Webb, and D. J. Shillington (2022). "Investigating short-period lake-generated microseisms using a broadband array of onshore and lake-bottom seismometers". *Seismological Research Letters* 93(3), pages 1585–1600. DOI: 10.1785/0220210155.

Ciacy, G. R. T. (1973). *Local lake microseisms recorded near Lake Taupō in the North Island of New Zealand*. URL: http://www.glodark.com/VP_app3.htm (visited on 06/01/2022).

Coffin, M. F., L. M. Gahagan, and L. A. Lauver (1997). *Present-day plate boundary digital data compilation*. Technical report. Institute for Geophysics.

Davy, B. (1993). "Seismic reflection profiling of the Taupo caldera, New Zealand". *Exploration Geophysics* 24(4), pages 443–454. DOI: 10.1071/eg993443.

De la Cruz-Reyna, S. and G. A. Reyes-Dávila (2001). "A model to describe precursory material-failure phenomena: applications to short-term forecasting at colima volcano, Mexico". *Bulletin of Volcanology* 63(5), pages 297–308. DOI: 10.1007/s004450100152.

Dmitrieva, K., A. J. Hotovec-Ellis, S. Prejean, and E. M. Dunham (2013). "Frictional-faulting model for harmonic tremor before Redoubt Volcano eruptions". *Nature Geoscience* 6(8), pages 652–656. DOI: 10.1038/ngeo1879.

Farrell, J., K. D. Koper, and R. A. Sohn (2023). "The Relationship Between Wind, Waves, Bathymetry, and Microseisms in Yellowstone Lake, Yellowstone National Park". *Journal of Geophysical Research: Solid Earth* 128(7), e2022JB025943. DOI: 10.1029/2022jb025943.

GeoNet (2022a). *Earthquake activity under Lake Taupō picks up. Volcanic Alert Level remains at Level 0.* Technical report TP – 2022/01. Lower Hutt, Wellington, New Zealand: GNS Science.

– (2022b). *Taupō Volcano: Volcanic Alert Level raised to Level 1. Ongoing earthquakes and deformation indicating minor volcanic unrest.* Technical report TP - 2022/04. Lower Hutt, Wellington, New Zealand: GNS Science.

– (2023). *Volcanic activity at Taupō Volcano is now back to background levels. The Volcanic Alert Level is lowered to Level 0.* Technical report TP - 2023/04. Lower Hutt, Wellington, New Zealand: GNS Science.

Gilmour, A. E. (1991). "Seiche characteristics in Lake Taupo, New Zealand (Note)". *New Zealand Journal of Marine and Freshwater Research*. DOI: 10.1080/00288330.1991.9516466.

Gómez M, D. M. and R. A. Torres C (1997). "Unusual low-frequency volcanic seismic events with slowly decaying coda waves observed at Galeras and other volcanoes". *Journal of Volcanology and Geothermal Research* 77(1-4), pages 173–193. DOI: 10.1016/s0377-0273(96)00093-5.

Green, D. N. and J. Neuberg (2006). "Waveform classification of volcanic low-frequency earthquake swarms and its implication at Soufrière Hills Volcano, Montserrat". *Journal of Volcanology and Geothermal Research* 153(1-2), pages 51–63. DOI: 10.1016/j.jvolgeores.2005.08.003.

Gualtieri, L., É. Stutzmann, V. Farra, Y. Capdeville, M. Schimmel, F. Ardhuin, and A. Morelli (2014). "Modelling the ocean site effect on seismic noise body waves". *Geophysical Journal International* 197(2), pages 1096–1106. DOI: 10.1093/gji/ggu042.

Hall, M. L., A. L. Steele, P. A. Mothes, and M. C. Ruiz (2013). "Pyroclastic density currents (PDC) of the 16–17 August 2006 eruptions of Tungurahua volcano, Ecuador: Geophysical registry and characteristics". *Journal of Volcanology and Geothermal Research* 265, pages 78–93. DOI: 10.1016/j.jvolgeores.2013.08.011.

Hasselmann, K. (1963). "A statistical analysis of the generation of microseisms". *Reviews of Geophysics* 1(2), pages 177–210. DOI: 10.1029/rg001i002p00177.

Ibáñez, J. and E. Carmona (2000). "Sismicidad volcánica". *Curso Internacional de Volcanología y Geofísica Volcánica, Serie Casa de los Volcanes* 7, pages 269–282.

Illsley-Kemp, F., S. J. Barker, C. J. N. Wilson, C. J. Chamberlain, S. Hreinsdóttir, S. Ellis, I. J. Hamling, M. K. Savage, E. R. H. Mestel, and F. B. Wadsworth (2021). "Volcanic unrest at Taupō volcano in 2019: Causes, mechanisms and implications". *Geochemistry, Geophysics, Geosystems* (e2021GC009803). DOI: 10.1029/2021gc009803.

Illsley-Kemp, F., P. Herath, C. J. Chamberlain, K. Michailos, and C. J. N. Wilson (2022). "A decade of earthquake activity at Taupō Volcano, New Zealand". *Volcanica* 5(2), pages 335–348. DOI: 10.30909/vol.05.02.335348.

Kerman, B. R. and R. F. Mereu (1993). "Wind-induced microseisms from Lake Ontario". *Atmosphere-Ocean* 31(4), pages 501–516. DOI: 10.1080/07055900.1993.9649483.

Kerman, B. R., R. F. Mereu, and D. Roy (1995). "Wind-induced microseisms from large lakes". *Sea Surface Sound'94*. World Scientific, pages 143–156. DOI: 10.1142/9789814447102_0010.

Konstantinou, K. I. and V. Schlindwein (2003). "Nature, wavefield properties and source mechanism of volcanic tremor: a review". *Journal of Volcanology and Geothermal Research* 119(1-4), pages 161–187. DOI: 10.1016/s0377-0273(02)00311-6.

Langridge, R. M., W. F. Ries, N. J. Litchfield, P. Villamor, R. J. Van Dissen, D. J. A. Barrell, M. S. Rattenbury, D. W. Heron, S. Haubrock, D. B. Townsend, J. M. Lee, K. R. Berryman, A. Nicol, S. C. Cox, and M. W. Stirling (2016). "The New Zealand Active Faults Database". *New Zealand Journal of Geology and Geophysics* 59(1), pages 86–96. DOI: 10.1080/00288306.2015.1112818.

Lara, L. E., J. A. Naranjo, and H. Moreno (2004). "Rhyodacitic fissure eruption in Southern Andes (Cordón Caulle; 40.5 S) after the 1960 (Mw: 9.5) Chilean earthquake: a structural interpretation". *Journal of Volcanology and Geothermal Research* 138(1-2), pages 127–138. DOI: 10.1016/j.jvolgeores.2004.06.009.

Latter, J. H. (1981). "Volcanic earthquakes, and their relationship to eruptions at Ruapehu and Ngauruhoe volcanoes". *Journal of Volcanology and Geothermal Research* 9(4), pages 293–309. DOI: 10.1016/0377-0273(81)90041-X.

Lesage, P., M. M. Mora, G. E. Alvarado, J. Pacheco, and J.-P. Métaxian (2006). "Complex behavior and source model of the tremor at Arenal volcano, Costa Rica". *Journal of Volcanology and Geothermal Research* 157(1-3), pages 49–59. DOI: 10.1016/j.jvolgeores.2006.03.047.

Linde, A. T. and I. S. Sacks (1998). "Triggering of volcanic eruptions". *Nature* 395(6705), pages 888–890. DOI: 10.1038/27650.

Longuet-Higgins, M. S. (1950). "A theory of the origin of microseisms". *Philosophical Transactions of the Royal Society of London. Series A, Mathematical and Physical Sciences* 243(857), pages 1–35. DOI: 10.1098/rsta.1950.0012.

Marple Jr, S. L. and W. M. Carey (1989). *Digital spectral analysis with applications*. Acoustical Society of America.

McNamara, D. E. and R. P. Buland (2004). "Ambient noise levels in the continental United States". *Bulletin of the Seismological Society of America* 94(4), pages 1517–1527. DOI: 10.1785/012003001.

McNutt, S. R. (2005). "Volcanic seismology". *Annual Review of Earth and Planetary Sciences* 32, pages 461–491. DOI: 10.1146/annurev.earth.33.092203.122459.

Mestel, E. R. H., B. Smith, K. Tapuke, F. Illsley-Kemp, L. Kaiser, D. Johnston, I. Connon, C. J. N. Wilson, G. S. Leonard, M. A. Clive, and M. K. Savage (2019). *Eruption or Catastrophe: Learning to Implement Preparedness for future Supervolcano Eruptions [Data set]*. DOI: 10.7914/SN/2B_2019.

Minakami, T. (1974). "Seismology of volcanoes in Japan". *Developments in Solid Earth Geophysics*. Volume 6. Elsevier, pages 1–27. DOI: 10.1016/B978-0-444-41141-9.50007-3.

Montegrossi, G., A. Farina, L. Fusi, and A. De Biase (2019). "Mathematical model for volcanic harmonic tremors". *Scientific Reports* 9(1), pages 1–14. DOI: 10.1038/s41598-019-50675-2.

Mori, J., H. Patia, C. McKee, I. Itikarai, P. Lowenstein, P. De Saint Ours, and B. Talai (1989). "Seismicity associated with eruptive activity at Langila volcano, Papua New Guinea". *Journal of Volcanology and Geothermal Research* 38(3-4), pages 243–255. DOI: 10.1016/0377-0273(89)90040-1.

Nabyl, A., J. Dorel, and M. Lardy (1997). "A comparative study of low-frequency seismic signals recorded at Stromboli volcano, Italy, and at Yasur volcano, Vanuatu". *New Zealand Journal of Geology and Geophysics* 40(4), pages 549–558. DOI: 10.1080/00288306.1997.9514783.

Norgaard, D. L., T. J. Parker, P. F. Cervelli, and D. Cervelli (2021). *Swarm*. DOI: 10.5066/P93A9MWK.

Pearson, K. (1895). "VII. Note on regression and inheritance in the case of two parents". *Proceedings of the Royal Society of London* 58(347-352), pages 240–242. DOI: 10.1098/rspl.1895.0041.

Peterson, J. R. (1993). "Observations and modeling of seismic background noise". *US Geological Survey Open-File Report* (93-322). DOI: 10.3133/ofr93322.

Potter, S. H., B. J. Scott, G. E. Jolly, D. M. Johnston, and V. E. Neall (2015). "A catalogue of caldera unrest at Taupo Volcanic Centre, New Zealand, using the volcanic unrest index (VUI)". *Bulletin of Volcanology* 77(9), pages 1–28. DOI: 10.1007/s00445-015-0956-5.

Seropian, G., B. M. Kennedy, T. R. Walter, M. Ichihara, and A. D. Jolly (2021). "A review framework of how earthquakes trigger volcanic eruptions". *Nature Communications* 12(1), pages 1–13. DOI: 10.1038/s41467-021-21166-8.

Smalls, P. T., R. A. Sohn, and J. A. Collins (2019). "Lake-bottom seismograph observations of microseisms in Yellowstone Lake". *Seismological Research Letters* 90(3), pages 1200–1208. DOI: 10.1785/0220180242.

Smith, K. and C. Tape (2019). "Seismic noise in central Alaska and influences from rivers, wind, and sedimentary basins". *Journal of Geophysical Research: Solid Earth* 124(11), pages 11678–11704. DOI: 10.1029/2019jb017695.

Soubestre, J., N. M. Shapiro, L. Seydoux, J. de Rosny, D. V. Droznin, S. Y. Droznina, S. L. Senyukov, and E. I. Gordeev (2018). "Network-based detection and classification of seismovolcanic tremors: Example from the Klyuchevskoy volcanic group in Kamchatka". *Journal of Geophysical Research: Solid Earth* 123(1), pages 564–582. DOI: 10.1002/2017jb014726.

Subira, J., J. Barrière, C. Caudron, A. Hubert-Ferrari, A. Oth, B. Smets, N. d'Oreye, and F. Kervyn (2023). "Detecting sources of shallow tremor at neighboring volcanoes in the Virunga Volcanic Province using seismic amplitude ratio analysis (SARA)". *Bulletin of Volcanology* 85(5), page 27. DOI: 10.1007/s00445-023-01640-5.

Van der Laat, L., M. M. Mora, J. F. Pacheco, P. Lesage, and E. Meneses (2022). "Seismicity during the recent activity (2009–2020) of Turrialba volcano, Costa Rica". *Journal of Volcanology and Geothermal Research*, page 107651. DOI: 10.1016/j.jvolgeores.2022.107651.

Watt, S. F. L., D. M. Pyle, and T. A. Mather (2009). "The influence of great earthquakes on volcanic eruption rate along the Chilean subduction zone". *Earth and Planetary Science Letters* 277(3-4), pages 399–407. DOI: 10.1016/j.epsl.2008.11.005.

Wilson, C. J. N., S. Blake, B. L. A. Charlier, and A. N. Sutton (2006). "The 26.5 ka Oruanui eruption, Taupo volcano, New Zealand: development, characteristics and evacuation of a large rhyolitic magma body". *Journal of Petrology* 47(1), pages 35–69. DOI: https://doi.org/10.1093/petrology/egi066.

Wilson, C. J. N. (1993). "Stratigraphy, chronology, styles and dynamics of late Quaternary eruptions from Taupo volcano, New Zealand". *Philosophical Transactions of the Royal Society of London. Series A: Physical and Engineering Sciences* 343(1668), pages 205–306. DOI: 10.1098/rsta.1993.0050.

Wilson, C. J. N. and B. L. A. Charlier (2009). "Rapid rates of magma generation at contemporaneous magma systems, Taupo Volcano, New Zealand: insights from U–Th model-age spectra in zircons". *Journal of Petrology* 50(5), pages 875–907. DOI: 10.1093/petrology/egp023.

Wilson, C. J. N. and J. V. Rowland (2016). "The volcanic, magmatic and tectonic setting of the Taupo Volcanic Zone, New Zealand, reviewed from a geothermal perspective". *Geothermics* 59, pages 168–187. DOI: 10.1016/j.geothermics.2015.06.013.

Xu, Y., K. D. Koper, and R. Burlacu (2017). "Lakes as a source of short-period (0.5–2 s) microseisms". *Journal of Geophysical Research: Solid Earth* 122(10), pages 8241–8256. DOI: 10.1002/2017jb014808.

Yukutake, Y., M. Miyazawa, R. Honda, M. Harada, H. Ito, M. Sakaue, K. Koketsu, and A. Yoshida (2013). "Remotely triggered seismic activity in Hakone volcano during and after the passage of surface waves from the 2011 M9. 0 Tohoku-Oki earthquake". *Earth and Planetary Science Letters* 373, pages 205–216. DOI: 10.1016/j.epsl.2013.05.004.

Zobin, V. M. (2011). *Introduction to volcanic seismology*. Volume 6. Elsevier. ISBN: 978-0-444-63631-7. DOI: https://doi.org/10.1016/C2015-0-00304-5.

Appendix A

The appendix contains details from the lake microseisms catalogue.

Table A1: Lake microseisms parameters at Taupō lake during 2019 using RATZ seismic station. *Start*: Start time of lake microseisms, *End*: End time of lake microseism, *Duration:* Duration of lake microseisms in hours.

ID	Start	End	Duration (h)
1	11/01/19 19:06	12/01/19 8:59	13
2	1/02/19 23:39	2/02/19 23:33	23
3	6/02/19 0:23	7/02/19 19:00	42
4	9/02/19 9:22	9/02/19 14:56	5
5	16/02/19 6:25	16/02/19 16:51	10
6	24/02/19 5:25	25/02/19 16:45	35
7	12/04/19 6:25	13/04/19 7:33	25
8	21/04/19 7:50	22/04/19 5:08	21
9	28/04/19 16:33	1/05/19 12:50	68
10	11/05/19 22:08	13/05/19 12:13	38
11	6/06/19 23:33	7/06/19 11:26	11
12	18/06/19 2:05	18/06/19 13:33	11
13	20/06/19 4:16	20/06/19 19:56	15
14	22/06/19 11:11	23/06/19 3:24	16
15	25/06/19 6:18	25/06/19 10:48	4
16	4/07/19 16:36	5/07/19 5:43	13
17	5/07/19 18:31	6/07/19 16:32	22
18	13/07/19 16:45	14/07/19 5:31	12
19	15/07/19 9:06	15/07/19 23:46	14
20	18/07/19 14:31	19/07/19 11:03	20
21	17/08/19 10:00	19/08/19 2:06	40
22	19/08/19 19:15	20/08/19 15:21	20
23	22/08/19 22:09	24/08/19 8:57	34
24	2/09/19 11:31	4/09/19 13:26	49
25	8/09/19 11:42	10/09/19 12:38	48
26	20/09/19 4:03	20/09/19 14:49	10
27	29/09/19 18:33	30/09/19 12:47	18
28	5/10/19 13:43	6/10/19 19:27	29
29	13/10/19 7:36	15/10/19 8:02	48
30	7/12/19 14:47	8/12/19 20:47	29
31	9/12/19 7:00	10/12/19 17:07	34
32	11/12/19 7:56	11/12/19 18:12	10
33	16/12/19 5:49	17/12/19 10:27	28
34	21/12/19 4:48	21/12/19 20:25	15
35	23/12/19 3:20	23/12/19 14:18	10
36	24/12/19 5:36	24/12/19 18:26	12
37	25/12/19 5:05	25/12/19 13:28	8
38	26/12/19 8:28	26/12/19 13:27	4

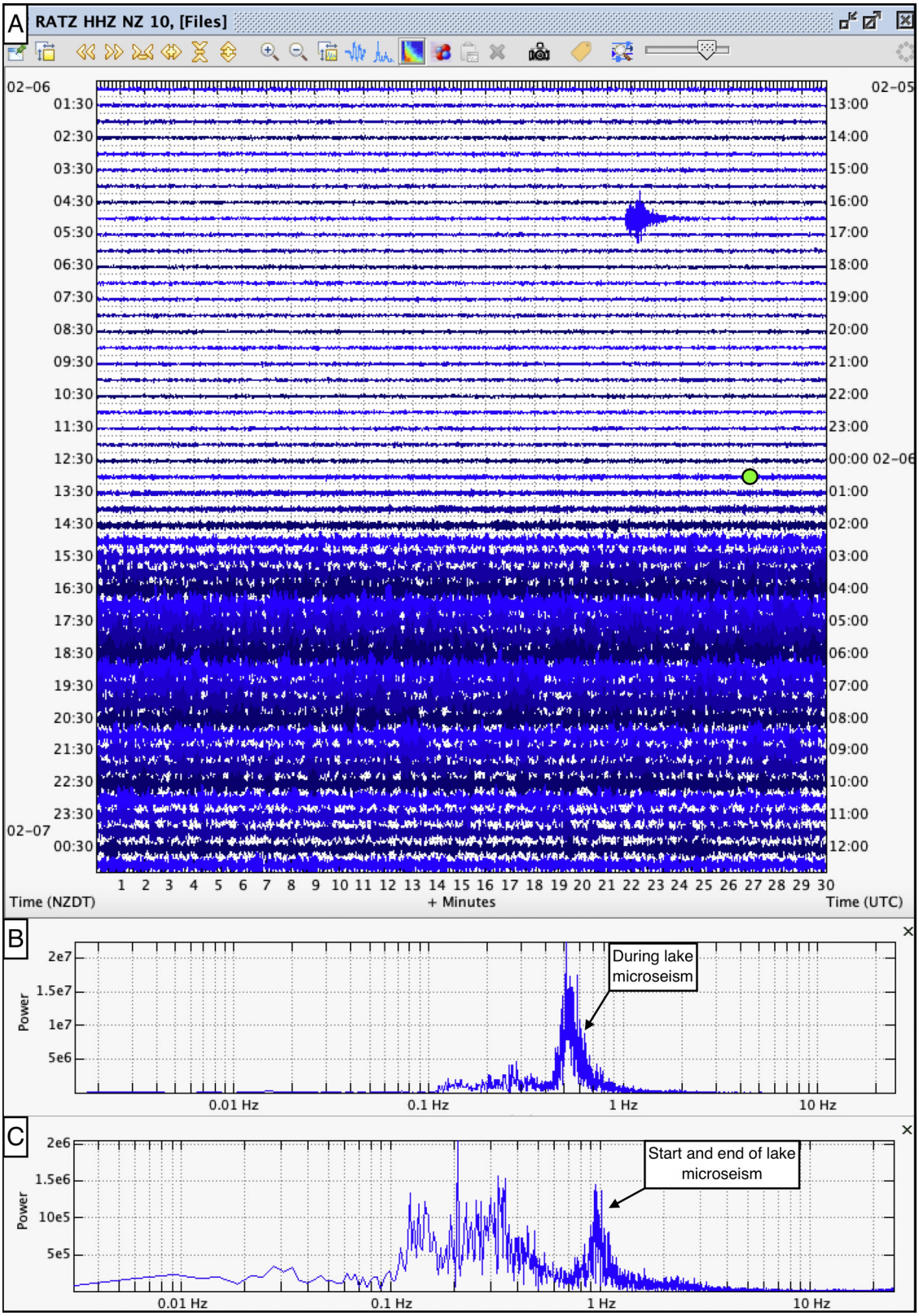

Figure A1: Illustration of the method used to identify the lake microseisms. [A] Helicorder of RATZ's vertical channel during February 2nd, 2019. The green points indicates the start of the lake microseisms. [B] During the occurrence of lake microseisms, the dominant frequency peak reaches up to 0.5 Hz in the spectrum. [C] The start of the lake microseisms is denoted when the frequency peak in the spectrum changes from a range of 0.7–1.0 Hz to 0.5 Hz, and ends with 0.7–1.0 Hz.

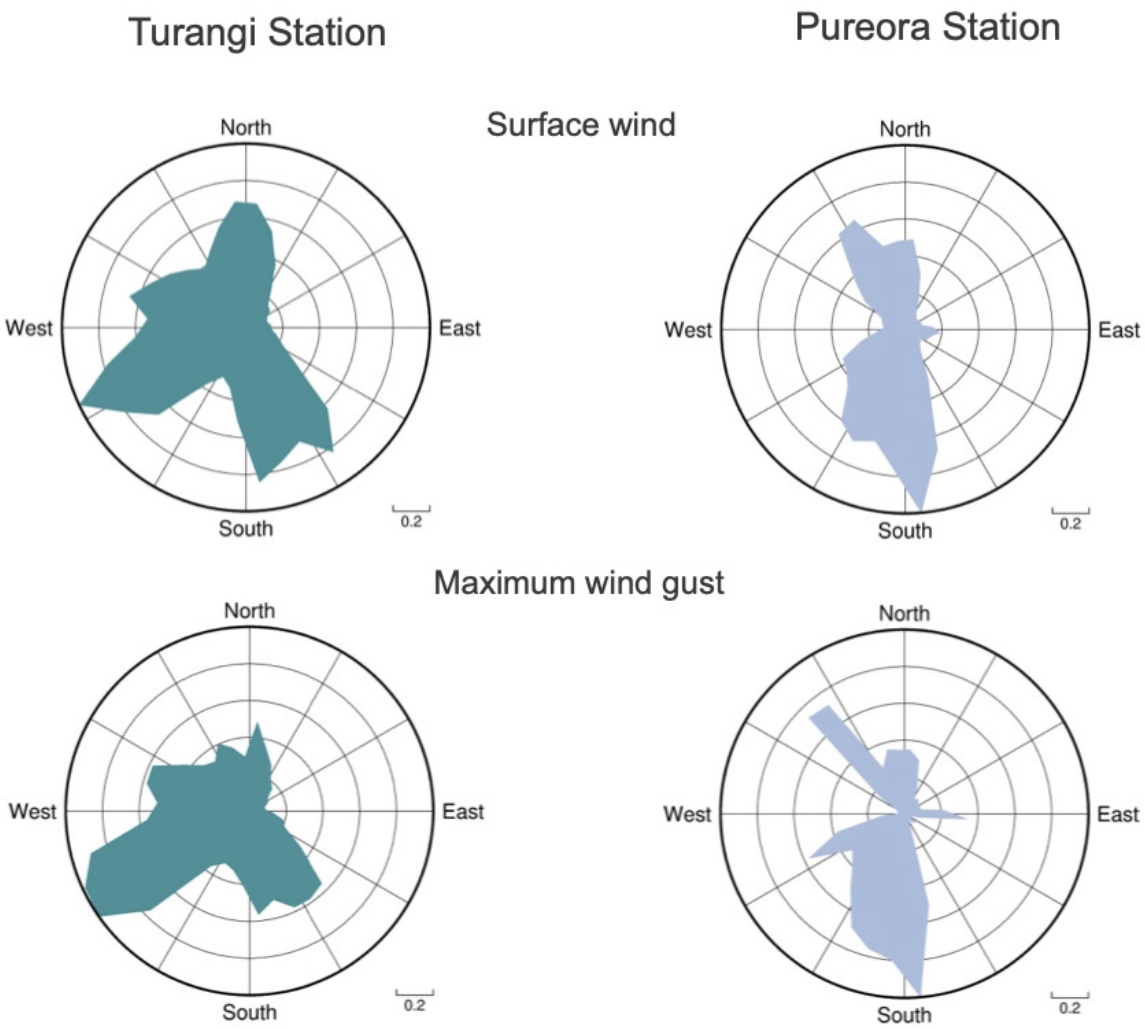

Figure A2: Preferential wind orientation at Tūrangi and Pureora stations during 2018–2019. In the first row, the preferential wind orientation of the surface wind, and the second row corresponds with preferential orientation of the maximum wind gust.

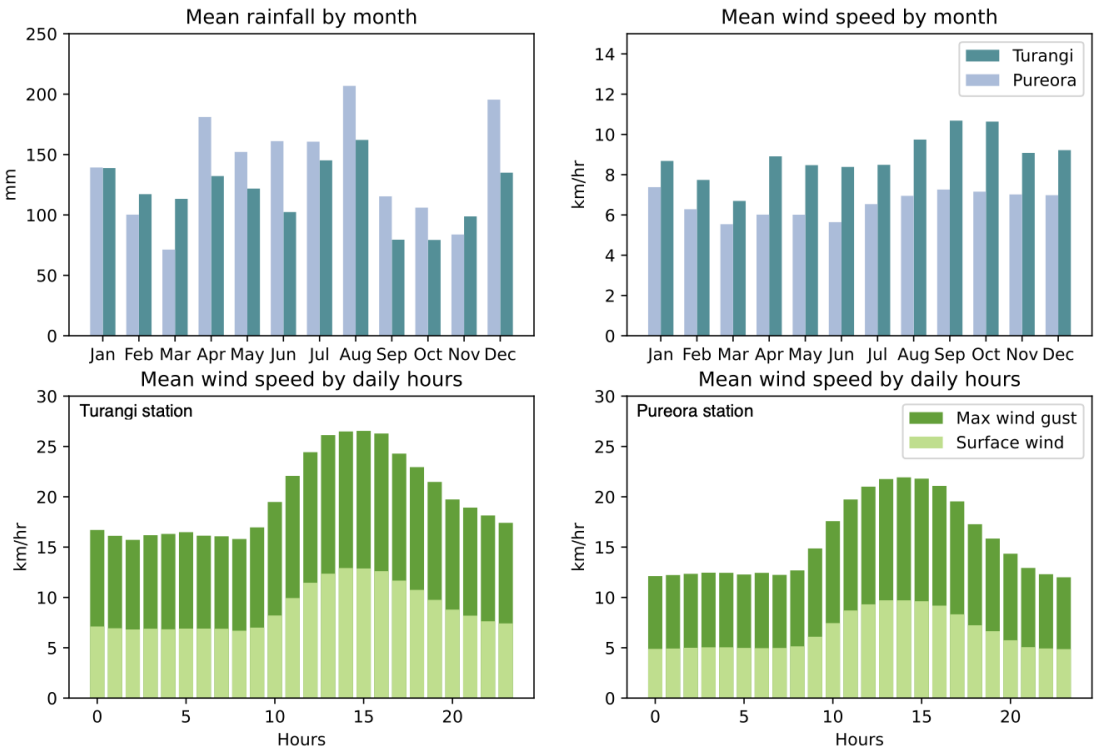

Figure A3: Mean cumulative precipitation and mean wind speed by month at Tūrangi and Pureora weather stations (top row). Hourly mean of maximum wind gust and surface wind at Tūrangi (lower left) and Pureora (lower right) with data from 2018–2019 (bottom row). Hours displayed in local time, where 0 represents midnight.